

3D Masked Autoencoders with Application to Anomaly Detection in Non-Contrast Enhanced Breast MRI

Daniel M. Lang^{1,2}, Eli Schwartz^{3,4}, Cosmin I. Bercea^{1,2}, Raja Giryes⁴, and Julia A. Schnabel^{1,2,5}
daniel.lang@tum.de

¹ Helmholtz Munich, Germany

² Technical University of Munich, Germany

³ IBM Research AI, Israel

⁴ Tel-Aviv University, Israel

⁵ King's College London, United Kingdom

Abstract. Self-supervised models allow (pre-)training on unlabeled data and therefore have the potential to overcome the need for large annotated cohorts. One leading self-supervised model is the masked autoencoder (MAE) which was developed on natural imaging data. The MAE is masking out a high fraction of visual transformer (ViT) input patches, to then recover the uncorrupted images as a pretraining task. In this work, we extend MAE to perform anomaly detection on breast magnetic resonance imaging (MRI). This new model, coined masked autoencoder for medical imaging (MAEMI) is trained on two non-contrast enhanced MRI sequences, aiming at lesion detection without the need for intravenous injection of contrast media and temporal image acquisition. During training, only non-cancerous images are presented to the model, with the purpose of localizing anomalous tumor regions during test time. We use a public dataset for model development. Performance of the architecture is evaluated in reference to subtraction images created from dynamic contrast enhanced (DCE)-MRI.

Keywords: Anomaly Detection · Masked Autoencoder · Unsupervised Learning.

1 Introduction

Annotation of medical data requires expert knowledge or labor-intensive testing methods, leading to high curation costs. Therefore, labeled medical imaging datasets are typically several orders of magnitude smaller than datasets generally encountered in computer vision. Deep learning networks require large amounts of data to be trained, making deployment of models in the medical domain cumbersome [4]. Self-supervised learning aims at model development in the absence of labeled examples and has the power to overcome those limiting factors [23]. A pretraining task is utilized to induce prior knowledge into the model, which

will then be fine-tuned for the respective downstream task of interest. One leading self-supervised approach is the masked autoencoder (MAE) [13], which was developed on natural imaging data. MAE is a transformer based autoencoder (AE) model that randomly removes a high fraction of its input patches, with the intention to recover the uncorrupted images as a self-supervised task.

In addition to constraints in data acquisition, medical datasets are also often highly imbalanced, featuring a skewed proportion of *healthy* and *unhealthy* examples. Anomaly detection (AD) models are designed to identify rare, uncommon elements that differ significantly from *normal* cases. In the medical domain, such models are employed to distinguish *abnormal* patterns of unhealthy examples from normal patterns of healthy cases.

Self-supervised anomaly detection combines both training strategies, aiming to identify abnormal cases without the requirement for labeled examples. This can be achieved by reconstruction-based methods [3,10]. Models are trained to recover their input, while restrictions on the architecture are applied. Such restrictions can be imposed by information bottlenecks [5] or the alteration of input images by application of noise [15,27] or removal of image parts [29,28]. During training, normal examples are shown to the model. In this way, the model is only able to reconstruct image parts stemming from the normal distribution reasonably well, while abnormal image parts result in higher error rates that can be utilized to generate anomaly maps during test time. Schwarz et al. [21] modified MAE to perform anomaly detection on natural imaging data. Most AD models in the area of medical imaging have been developed on MRI of the brain, e.g. [1,2,15]. Further areas of application include, e.g. chest X-ray, optical coherence tomography (OCT) and mammography [25].

We aim at model development on breast MRI, which is the most sensitive breast cancer imaging method [16], applied for tumor staging but also cancer screening. DCE-MRI refers to the acquisition of images before, during and after intravenous injection of contrast media, which improves the signal intensity of neoangiogenically induced vascular changes that allows for better detection of lesions [26]. However, long scan times and high costs limit widespread use of the technique, leading different studies to investigate the ability to abbreviate *contrast enhanced* breast MRI protocols [16]. We demonstrate the capability of self-supervised models for anomaly detection on *non-contrast enhanced* breast MRI, which reduces the number of required image sequences dramatically and therefore results in even faster image acquisition. Moreover, no intravenous injection of contrast media is needed, which is known to be able to cause side effects [12].

Contribution In this work we remodel MAE and extended and further develop the approach of Schwarz et al. [21], enabling self-supervised anomaly detection on 3D multi-spectral medical imaging data. To do so, we advance the definition of input patches and positional embedding of the ViT architecture and refine the random masking strategy of He et al. [13]. We then train the model on non-contrast enhanced breast MRI. During training only healthy, non-cancerous

breast MRIs are shown to the model, aiming to identify breast lesions as anomalies during test time. To the best of our knowledge, we are the first to make the following contributions:

- We extend and further refine MAEs to perform anomaly detection on 3D multi-spectral medical imaging.
- We investigate the capability of self-supervised anomaly detection to identify pathologies in breast MRI.
- We assess the performance of anomaly detection algorithms in reference to DCE-MRI subtraction images. Paving the way for a more widespread use of MRI in breast cancer diagnosis.

2 Related Work

The ability of deep convolutional AEs to perform reconstruction based self-supervised anomaly detection on imaging data has been investigated by several studies, see e.g. [1,2,22]. *Kascenas et al.* [15] trained a denoising AE on brain MRI, such that unhealthy pathologies were removed during test time. *Zavrtanik et al.* [29] developed a convolutional AE, masking part of the input to perform inpainting on natural imaging and video data.

MAE has been developed on 2D natural images, to be finetuned on a classification problem. In the context of classification the approach has been modified in several different ways. *Feichtenhofer et al.* [9] enhanced the model to do classification on natural video data.

Prabhakar et al. [18] improved the initial MAE architecture, by incorporation of a contrastive and a auxiliary loss term, to perform classification on brain MRI. Our model relies on image reconstruction and computation of a voxel-wise difference in the downstream task. Therefore, we use unaltered mean squared error (MSE) as a loss.

Due to its high masking ratio, anomalies are likely to be removed by MAE. Which led *Tian et al.* [24] to employ the model on anomaly detection in 2D colonoscopy and X-ray data. They introduced *memory-augmented self-attention* and a *multi-level cross-attention operator* in the underlying ViT architecture, to limit dependency on random masking. In contrast, we train our model on multi-spectral 3D data following the principle strategy of *Schwartz et al.* [21]. The approach does not rely on any modifications in the ViT architecture, and maximizes the likelihood for the anomaly to be removed by application of a high number of random masks. We extend and further develop the model trained on natural imaging data to be able to handle multi-spectral volumetric medical imaging data.

MAE based anomaly detection models employ a problem independent pre-training task, recovering pseudo-normal images from the masked input. Denoising autoencoders (DAEs) used for AD are aiming to achieve the same effect by pretraining on noise removal. However, selection of noise has to fit the distribution of possible anomalies for the approach to succeed. Hence, a model trained

on one specific task is very unlikely to succeed reasonably well in another problem setting. In contrast to that, the ability of MAE based anomaly detection to succeed in modified settings has been proven by [21], achieving state of the art (SOTA) performance on few- and zero-shot problems.

Identification of lesions in breast MRI has only been performed by *supervised* models so far. *Maicas et al.* [17] trained a deep Q-network for breast lesion detection, *Ayatollahi et al.* modified RetinaNet and *Herent et al.* [14] utilized a 2D ResNet50. Notably, all of those approaches were trained on DCE-MRI data, relying on injection of contrast media. Whereas, we perform self-supervised anomaly detection on non-contrast enhanced MRI.

3 Dataset

We use the public Duke-Breast-Cancer-MRI cohort [19,20] from The Cancer Imaging Archive [7]. The set includes axial breast MRI data of 922 patients comprising a non-fat saturated pre-contrast T1-weighted sequence, a fat-saturated T1-weighted pre-contrast sequence and several post-contrast fat-saturated T1-weighted sequences. Tumor lesion annotations were given in the form of bounding boxes. Furthermore, a U-Net model for generation of breast tissue masks was provided [6]. All images were standardized to the same voxel spacing of $0.75mm \times 0.75mm \times 1.0mm$, cropped to involve the chest area only, and normalized to a mean and standard deviation value of 0.5 and 0.25 per image. Cases involving bilateral breast cancer were removed from the cohort. Thus, each of the remaining patients exhibited one breast that contained a tumor lesion, treated as *abnormal/unhealthy*, and another breast not affected by cancer, treated as *normal/healthy*. The dataset was split into a training set of 745 patients, a validation set of 50 patients and a test set of 100 patients. Notably, no *normal - abnormal* pairs of the same patient were involved in different datasets. Due to the high memory requirements of transformer models, MRI-patches of size $240 \times 168 \times 8$ voxels in lateral-posterior-superior (LPS) directions were cropped from both MRI sequences to be then divided into ViT-patches and processed by the encoder.

Following clinical routine, subtraction images S between the image acquired before I_{pre} and all of the m images acquired after injection of contrast media I_{post}^k were computed:

$$S = \frac{1}{m} \sum_{k=0}^m (I_{\text{pre}} - I_{\text{post}}^k)^2 * \text{min}_{3 \times 3 \times 2}, \quad (1)$$

with a minimum filter of size $3 \times 3 \times 2$ applied for noise removal.

4 Method

A scheme of our model can be seen in Figure 1. We modified the ViT architecture

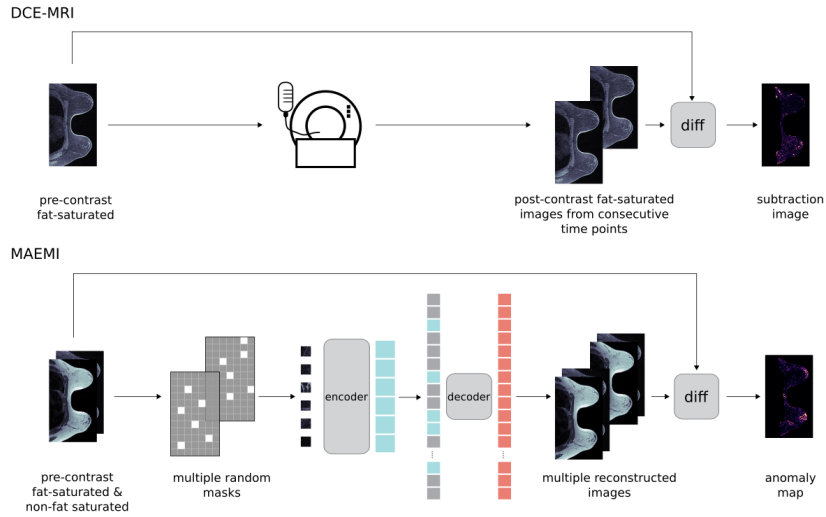


Fig. 1. DCE-MRI imaging vs. MAEMI. For DCE-MRI, several MRIs before, during and after injection of contrast media are acquired. MAEMI uses different random masks for generation of pseudo-healthy recovered images. Both methods construct error maps by calculation of the mean squared error difference between each of the post-contrast/reconstructed images with the pre-contrast/ uncorrupted image.

of [8] to 3D multispectral MRI, i.e. the positional embedding and definition of ViT-patches was redefined and enhanced to incorporate a third dimension. This 3D-ViT was then embedded in the MAE approach of [13]. To do so, generation of mask tokens and random masking of ViT-patches had to be remodeled. The approach coined masked autoencoder for medical imaging (MAEMI) uses a 3D-ViT with 12 transformer blocks and a embedding dimension of 768 as encoder while for the decoder a embedding dimension of 384 and a depth of 4 has been chosen.

In addition, we further improved the anomaly detection model of [21]. MRIs were processed by patches, such that memory requirements of the transformer based architecture could be reduced, enabling exploitation of whole MRI volumes. A overlapping patch scheme has been chosen, in order to reduce artifacts on patch borders. Anomaly maps were generated from two input sequences, i.e. non-fat saturated (NFS) and fat saturated (FS).

Error maps per input sequence E_i^{seq} were constructed by the MSE between the reconstructed patches R_i^{seq} and the unmasked MRI-patch I^{seq} :

$$E_i^{\text{seq}} = (I^{\text{seq}} - R_i^{\text{seq}})^2 * \min_{3 \times 3 \times 2}, \quad (2)$$

with a minimum filter of size $3 \times 3 \times 2$ applied for further reduction of artifacts. On a voxel level, final error scores were computed by the mean value of all patch predictions. Error maps of both multi-spectral input sequences, NFS and FS,

were then summed up and convolved with the same minimum filter as before:

$$E = \frac{1}{2} (E^{\text{NFS}} + E^{\text{FS}}) * \text{min}_{3 \times 3 \times 2}, \quad (3)$$

for generation of a final MR image level anomaly map.

Training Specifics During training, only MRI-patches of healthy breasts, containing no tumor lesions, were shown to the model with patches being cropped randomly. In addition to random cropping, random flipping on the coronal and sagittal plane was applied as a augmentation technique during training. A batch size of 6 and a learning rate of 10^{-3} were applied. Each model was trained for 1000 epochs, with the number of warm up epochs [11] set to 7. Weights of the trained model of [13], developed on ImageNet, were used to initialize the transformer layers in the encoder, while weights of the encoding layer and the decoder were randomly initialized. During test time a stride of size $64 \times 42 \times 2$ performing 6 repetitions was used to process whole MRI volumes.

Metrics We used voxel wise area under the receiver operating characteristics curve (AUROC) and average precision (AP) as performance measures. Only voxels lying inside the breast tissue segmentation mask were taken into account for computation, as injection of contrast media leads also to an uptake in tissue lying outside the breast area, ref. Figure 5 the Supplemental Materials. However, for AP one has to consider the large imbalance between normal and abnormal tissue labels, leading to an expected small baseline performance. Moreover, ground truth annotations were only given in the form of bounding boxes, depicting only a rough delineation of tumor tissue with several ground truth true positive (TP) scores involved that should in fact be true negative (TN). This has an higher impact on AP than on AUROC, as TP scores are involved in precision and recall but not in the false positive rate (FPR) of the ROC, which also takes TN labels into account.

5 Results

ViT-patch size and masking ratio have been varied for hyperparameter tuning. The best performing model featured a masking ratio of 90% and a ViT-patch size of $8 \times 8 \times 2$, AUROC and AP results are shown in Table 1. Example results are shown in Figure 2. Mean baseline performance of the AP measure, given by the number of voxels inside the bounding box divided by the number of voxels lying inside the breast tissue segmentation mask, was given by 0.046.

Ablation Studies We studied the influence of the patch size and masking ratio on model performance. Figure 3 presents the dependency of AUROC and AP on the masking ratio for a fixed ViT-patch size of $8 \times 8 \times 2$. Dependency on ViT-patch size for a fixed masking ratio of 90% is given in Table 2. The Nvidia RTX A6000 used for training, featuring 48 GB of memory, only allowed for a smallest size of $8 \times 8 \times 2$. Therefore, the slice dimension of ViT-patches was fixed at a value of 4 pixels, probing only different axial sizes.

Table 1. MAEMI achieves a higher AUROC, while DCE-MRI features a higher AP. However, significance of AP results are limited (see Section 4).

	AUROC	AP
MAEMI	0.732	0.081
DCE-MRI	0.705	0.127

Table 2. Ablation study on different (axial) ViT-patch sizes, for a fixed masking ratio of 90%. Smaller patch sizes lead to higher performance.

ViT-patch size	AUROC	AP
$6 \times 6 \times 4$	0.724	0.0784
$8 \times 8 \times 4$	0.712	0.0777
$12 \times 12 \times 4$	0.660	0.0750
$24 \times 24 \times 4$	0.546	0.0560

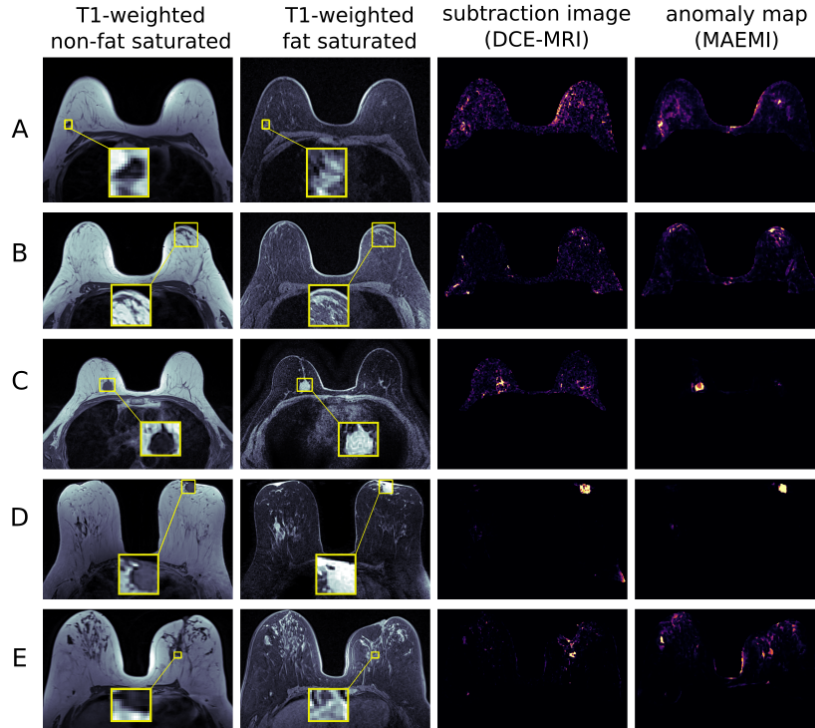


Fig. 2. Example results. The first two columns show the non-contrast enhanced images used as an input to the anomaly detection model, and the last two columns present subtraction images generated by DCE-MRI and anomaly detection maps generated by MAEMI, respectively. For patients in rows A, B and C, anomaly maps show superior performance over subtraction images. For patient D, both methods are able to identify the pathology. For patient E, our model only detects the borders of the pathology, while the subtraction image identifies the lesion.

MAEMI for Anomaly Detection in Breast MRI

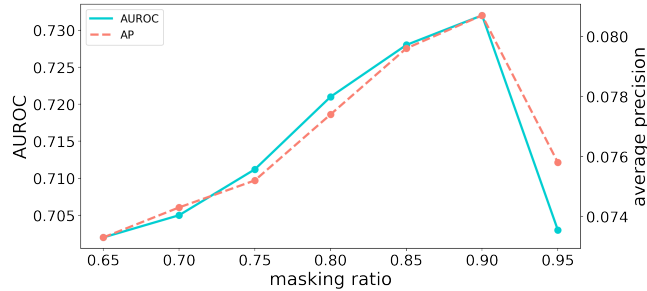


Fig. 3. Ablation study on the masking ratio for a fixed ViT-patch size of $8 \times 8 \times 2$. High masking ratios lead to better performance, with an optimum reached at 90%. Afterwards, performance suffers from a steep decline.

6 Discussion

We developed a new transformer-based AE model that can be trained on multi-spectral volumetric medical imaging data. We have applied our model to anomaly detection on non-contrast enhanced breast MRI. Model performance was at the same level as for DCE-MRI generated subtraction images. Thus, we were able to demonstrate the general ability for automated identification of suspicious pathologies on non-contrast enhanced breast MRI.

MAEMI achieved a higher AUROC while DCE-MRI generated subtraction images resulting in better AP performance. Limitations of evaluation metrics due to ground truth labels given in the form of bounding boxes were stated in Section 4. Determination of an optimal performance measure for ground truth bounding boxes in the case of unsupervised anomaly detection remains an active area of research.

We found an optimal masking ratio of 90% for our model. *Feichtenhofer et al.* [9] identified the same ratio to work best for video classification. However, masking plays a significantly different role for MAE architectures utilized for anomaly detection, with ViT-patch removal not only applied during training but also during test time. *Tian et al.* [24] employed the standard masking ratio of 75% for their model, trained to identify pathologies on 2D X-ray and colonoscopy data and did not report any ablation studies.

Automated generation of anomaly maps from non-contrast enhanced imaging allows for identification of suspicious lesions without the need for temporal imaging, which results in a drastic reduction of costs and acquisition time, two major factors limiting widespread application of MRI in breast cancer screening [16]. Therefore, we paved the way for a more widespread application of MRI in breast cancer diagnosis. Furthermore, patients can potentially be spared from intravenous injection of contrast media, which is known to be able to cause side effects [12]. Clinical differences and benefits between MAEMI and DCE-MRI will still need to be investigated in a larger clinical study.

Data Use Declaration All data used for this study is publicly available from The Cancer Imaging Archive [19,7] under the [CC BY-NC 4.0](#) license.

Supplementary Material

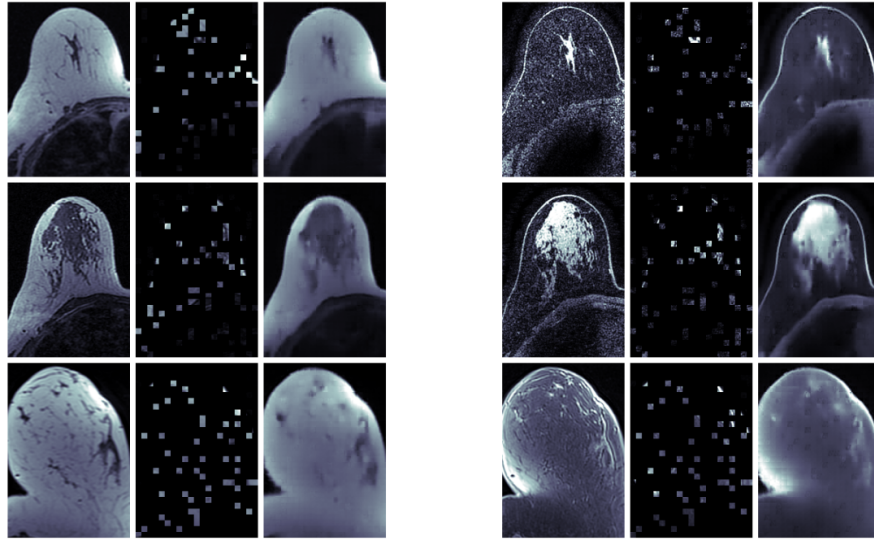


Fig. 4. Reconstruction examples. The left block shows axial slices of T1 non-fat saturated MRI-patches and the right block T1 fat saturated slices. The first column shows unaltered MRI-patches, the second column the masked model input and the third column the MRI-patches recovered by MAEMI. Examples represent a masking ratio of 90% (for the whole 3D patch) and a ViT-patch size of $8 \times 8 \times 2$.

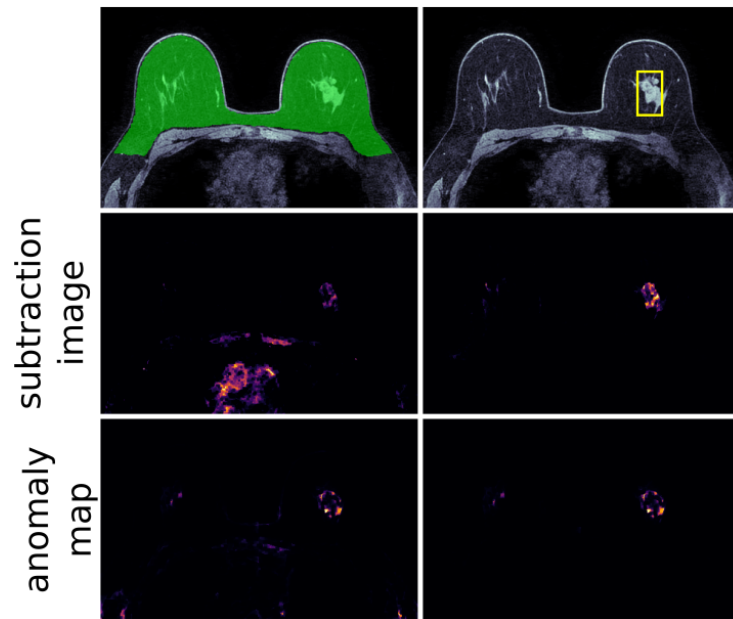


Fig. 5. Subtraction images and anomaly maps were multiplied with segmentation masks to remove anomalies lying obviously outside of the breast tissue. This is mainly needed as contrast agent is also taken up in organs outside the breast. The left column shows the raw subtraction/anomaly map, and the right column the raw maps multiplied with the segmentation mask of the image in the upper left corner. Performance metrics were only calculated for voxels lying inside the segmentation mask, limiting the influence of trivial predictions, i.e. voxels that represent air do not containing any anomalies.

References

1. Baur, C., Denner, S., Wiestler, B., Navab, N., Albarqouni, S.: Autoencoders for unsupervised anomaly segmentation in brain MR images: a comparative study. *Medical Image Analysis* **69**, 101952 (2021)
2. Bercea, C.I., Wiestler, B., Rueckert, D., Albarqouni, S.: Federated disentangled representation learning for unsupervised brain anomaly detection. *Nature Machine Intelligence* **4**(8), 685–695 (2022)
3. Bergmann, P., Löwe, S., Fauser, M., Sattlegger, D., Steger, C.: Improving unsupervised defect segmentation by applying structural similarity to autoencoders. *arXiv preprint arXiv:1807.02011* (2018)
4. Ching, T., Himmelstein, D.S., Beaulieu-Jones, B.K., Kalinin, A.A., Do, B.T., Way, G.P., Ferrero, E., Agapow, P.M., Zietz, M., Hoffman, M.M., et al.: Opportunities and obstacles for deep learning in biology and medicine. *Journal of The Royal Society Interface* **15**(141), 20170387 (2018)
5. Chow, J.K., Su, Z., Wu, J., Tan, P.S., Mao, X., Wang, Y.H.: Anomaly detection of defects on concrete structures with the convolutional autoencoder. *Advanced Engineering Informatics* **45**, 101105 (2020)
6. Chris, L.: 3D-Breast-FGT-and-Blood-Vessel-Segmentation. <https://github.com/mazurowski-lab/3D-Breast-FGT-and-Blood-Vessel-Segmentation> (2022)
7. Clark, K., Vendt, B., Smith, K., Freymann, J., Kirby, J., Koppel, P., Moore, S., Phillips, S., Maffitt, D., Pringle, M., et al.: The Cancer Imaging Archive (TCIA): maintaining and operating a public information repository. *Journal of digital imaging* **26**, 1045–1057 (2013)
8. Dosovitskiy, A., Beyer, L., Kolesnikov, A., Weissenborn, D., Zhai, X., Unterthiner, T., Dehghani, M., Minderer, M., Heigold, G., Gelly, S., et al.: An image is worth 16x16 words: Transformers for image recognition at scale. *arXiv preprint arXiv:2010.11929* (2020)
9. Feichtenhofer, C., Fan, H., Li, Y., He, K.: Masked autoencoders as spatiotemporal learners. *arXiv preprint arXiv:2205.09113* (2022)
10. Gong, D., Liu, L., Le, V., Saha, B., Mansour, M.R., Venkatesh, S., Hengel, A.v.d.: Memorizing normality to detect anomaly: Memory-augmented deep autoencoder for unsupervised anomaly detection. In: *Proceedings of the IEEE/CVF International Conference on Computer Vision*. pp. 1705–1714 (2019)
11. Goyal, P., Dollár, P., Girshick, R., Noordhuis, P., Wesolowski, L., Kyrola, A., Tulloch, A., Jia, Y., He, K.: Accurate, large minibatch sgd: Training imagenet in 1 hour. *arXiv preprint arXiv:1706.02677* (2017)
12. Hasebroock, K.M., Serkova, N.J.: Toxicity of MRI and CT contrast agents. *Expert opinion on drug metabolism & toxicology* **5**(4), 403–416 (2009)
13. He, K., Chen, X., Xie, S., Li, Y., Dollár, P., Girshick, R.: Masked autoencoders are scalable vision learners. In: *Proceedings of the IEEE/CVF Conference on Computer Vision and Pattern Recognition*. pp. 16000–16009 (2022)
14. Herent, P., Schmauch, B., Jehanno, P., Dehaene, O., Saillard, C., Balleyguier, C., Arfi-Rouche, J., Jégou, S.: Detection and characterization of MRI breast lesions using deep learning. *Diagnostic and interventional imaging* **100**(4), 219–225 (2019)
15. Kascenas, A., Pugeault, N., O’Neil, A.Q.: Denoising autoencoders for unsupervised anomaly detection in brain MRI. In: *International Conference on Medical Imaging with Deep Learning*. pp. 653–664. PMLR (2022)
16. Leithner, D., Moy, L., Morris, E.A., Marino, M.A., Helbich, T.H., Pinker, K.: Abbreviated MRI of the breast: does it provide value? *Journal of Magnetic Resonance Imaging* **49**(7), e85–e100 (2019)

17. Maicas, G., Carneiro, G., Bradley, A.P., Nascimento, J.C., Reid, I.: Deep reinforcement learning for active breast lesion detection from DCE-MRI. In: Medical Image Computing and Computer Assisted Intervention- MICCAI 2017: 20th International Conference, Quebec City, QC, Canada, September 11-13, 2017, Proceedings, Part III. pp. 665–673. Springer (2017)
18. Prabhakar, C., Li, H.B., Yang, J., Shit, S., Wiestler, B., Menze, B.: ViT-AE++: Improving Vision Transformer Autoencoder for Self-supervised Medical Image Representations. arXiv preprint arXiv:2301.07382 (2023)
19. Saha, A., Harowicz, M., Grimm, L., Weng, J., Cain, E., Kim, C., Ghate, S., Walsh, R., Mazurowski, M.: Dynamic contrast-enhanced magnetic resonance images of breast cancer patients with tumor locations. *The Cancer Imaging Archive* (2021)
20. Saha, A., Harowicz, M.R., Grimm, L.J., Kim, C.E., Ghate, S.V., Walsh, R., Mazurowski, M.A.: A machine learning approach to radiogenomics of breast cancer: a study of 922 subjects and 529 DCE-MRI features. *British journal of cancer* **119**(4), 508–516 (2018)
21. Schwartz, E., Arbelle, A., Karlinsky, L., Harary, S., Scheidegger, F., Doveh, S., Giryes, R.: MAEDAY: MAE for few and zero shot Anomaly-Detection. arXiv preprint arXiv:2211.14307 (2022)
22. Somepalli, G., Wu, Y., Balaji, Y., Vinzamuri, B., Feizi, S.: Unsupervised anomaly detection with adversarial mirrored autoencoders. In: *Uncertainty in Artificial Intelligence*. pp. 365–375. PMLR (2021)
23. Sun, C., Shrivastava, A., Singh, S., Gupta, A.: Revisiting unreasonable effectiveness of data in deep learning era. In: *Proceedings of the IEEE international conference on computer vision*. pp. 843–852 (2017)
24. Tian, Y., Pang, G., Liu, Y., Wang, C., Chen, Y., Liu, F., Singh, R., Verjans, J.W., Carneiro, G.: Unsupervised anomaly detection in medical images with a memory-augmented multi-level cross-attentional masked autoencoder. arXiv preprint arXiv:2203.11725 (2022)
25. Tschuchnig, M.E., Gadermayr, M.: Anomaly detection in medical imaging—a mini review. In: *Data Science—Analytics and Applications: Proceedings of the 4th International Data Science Conference—iDSC2021*. pp. 33–38. Springer (2022)
26. Turnbull, L.W.: Dynamic contrast-enhanced MRI in the diagnosis and management of breast cancer. *NMR in Biomedicine: An International Journal Devoted to the Development and Application of Magnetic Resonance In Vivo* **22**(1), 28–39 (2009)
27. Wyatt, J., Leach, A., Schmon, S.M., Willcocks, C.G.: AnoDDPM: Anomaly Detection With Denoising Diffusion Probabilistic Models Using Simplex Noise. In: *Proceedings of the IEEE/CVF Conference on Computer Vision and Pattern Recognition (CVPR) Workshops*. pp. 650–656 (June 2022)
28. Yan, X., Zhang, H., Xu, X., Hu, X., Heng, P.A.: Learning semantic context from normal samples for unsupervised anomaly detection. In: *Proceedings of the AAAI Conference on Artificial Intelligence*. vol. 35, pp. 3110–3118 (2021)
29. Zavrtnik, V., Kristan, M., Skočaj, D.: Reconstruction by inpainting for visual anomaly detection. *Pattern Recognition* **112**, 107706 (2021)